

## Lanthanide level location and charge carrier trapping in $\text{LiLnSiO}_4:\text{Ce}^{3+},\text{Sm}^{3+}$ , Ln = Y or Lu

This article has been downloaded from IOPscience. Please scroll down to see the full text article.

2006 J. Phys.: Condens. Matter 18 4503

(<http://iopscience.iop.org/0953-8984/18/19/006>)

View [the table of contents for this issue](#), or go to the [journal homepage](#) for more

Download details:

IP Address: 129.252.86.83

The article was downloaded on 28/05/2010 at 10:39

Please note that [terms and conditions apply](#).

# Lanthanide level location and charge carrier trapping in $\text{LiLnSiO}_4:\text{Ce}^{3+}$ , $\text{Sm}^{3+}$ , $\text{Ln} = \text{Y}$ or $\text{Lu}$

A V Sidorenko<sup>1</sup>, P Dorenbos<sup>1</sup>, A J J Bos<sup>1</sup>, C W E van Eijk<sup>1</sup> and P A Rodnyi<sup>2</sup>

<sup>1</sup> Delft University of Technology, Faculty of Applied Sciences, Mekelweg 15, 2629 JB Delft, Netherlands

<sup>2</sup> Politechnical University, Politehnicheskaya 29, 195251 St-Petersburg, Russia

E-mail: [p.dorenbos@tudelft.nl](mailto:p.dorenbos@tudelft.nl)

Received 6 January 2006

Published 25 April 2006

Online at [stacks.iop.org/JPhysCM/18/4503](http://stacks.iop.org/JPhysCM/18/4503)

## Abstract

By doping an inorganic compound with two specific types of trivalent rare-earth impurities the controlled creation of electron- and hole-trapping centres is possible. This is demonstrated with experimental data on  $\text{LiLnSiO}_4:\text{Ce}^{3+}$ ,  $\text{Sm}^{3+}$ ,  $\text{Ln} = \text{Y}$  or  $\text{Lu}$ . After exposure to ionizing radiation electrons are captured by  $\text{Sm}^{3+}$  and holes are captured by  $\text{Ce}^{3+}$ . The electron trapping depth is given by the energy difference between the  $\text{Sm}^{2+}$  ground state and the bottom of the conduction band. This energy is estimated from the energy of charge transfer from the valence band to  $\text{Eu}^{3+}$  employing recently developed models. The trapping energy is also determined from thermoluminescence studies. Both values are in good agreement.

## 1. Introduction

When an inorganic compound after a previously given radiation dose is slowly heated it often shows visible luminescence when specific temperatures are reached. This phenomenon is known as thermoluminescence and the recorded luminescence as function of temperature is called a glow curve. Such a curve generally displays several glow peaks, each of them caused by thermally activated release of charge carriers (electrons and/or holes) from charge traps in the compound. The released carriers recombine at luminescence centres, giving rise to the glow. Glow curve analysis provides charge trapping parameters like the depth of the charge trap, the attempt-to-escape frequency for trap escape, and the number of trapped charge carriers [1]. Thermoluminescence analysis is often used as a tool, for example for dosimetry, without precise knowledge of the nature of the underlying charge traps. The type of defects that are associated with the trapping centres and even whether they are hole traps or electron traps is usually not known.

Trivalent and divalent lanthanide ions give rise to occupied and unoccupied levels in the forbidden band of inorganic compounds. When the ground state of a lanthanide ion is located above the top of the valence band it can capture a hole from that valence band. The trapping depth is given by the energy difference between the ground state and the top of that band. A trivalent lanthanide can capture an electron from the conduction band when the energy of the ground state of the then created divalent lanthanide is located below the bottom of the conduction band. The trapping depth is equal to the energy difference between the bottom of the conduction band and the ground state of the divalent lanthanide ion.

It is well known that  $\text{Eu}^{2+}$ ,  $\text{Ce}^{3+}$ , and  $\text{Tb}^{3+}$  as dopants in compounds often act as hole traps whereas  $\text{Sm}^{3+}$  and  $\text{Eu}^{3+}$  act as electron traps. For example, the alkaline earth sulfides doped with the combination  $\text{Eu}^{2+}$  and  $\text{Sm}^{3+}$  or the combination  $\text{Ce}^{3+}$  and  $\text{Eu}^{3+}$  were intensively studied for their charge storage properties under optical or ionizing radiation excitation, and the materials were considered for optical data storage applications [2–11]. However, quantitative data on the location of electron trapping and electron donating levels were not published.

Precise knowledge on the level location of lanthanide impurities in compounds has been lacking for many decades. However, recently techniques and models to determine these became available. By means of resonant photoelectron emission studies Thiel *et al* [12] determined the systematic behaviour in the 4f ground state energy of trivalent lanthanides relative to the valence band in various compounds. Another approach is based on the energy needed to transfer an electron from the valence band to  $\text{Eu}^{3+}$ , which provides the ground state position of  $\text{Eu}^{2+}$ . These approaches were further developed by one of us, and it is now possible to make approximate level schemes for all divalent and all trivalent lanthanides in compounds with relatively few spectroscopic parameters [13].

The goal of this paper is to demonstrate how the depth of electron trapping by trivalent lanthanide ions can be determined by combining spectroscopic and thermo-luminescence data. With these new methods we can now assign glow peaks to specific lanthanide defects. This work is divided into three parts. The first is dedicated to experimental determination of the parameters required to determine the absolute location of lanthanide energy levels in  $\text{LiYSiO}_4$  and  $\text{LiLuSiO}_4$ . The second is devoted to the elucidation of the nature of trapping defects in these phosphors. In the final part the results are compared, and a consistent model for the storage and recombination mechanism in lanthanide doped  $\text{LiYSiO}_4$  and  $\text{LiLuSiO}_4$  is constructed.

## 2. Experimental details

Samples of  $\text{LiLn}_{1-x-y}\text{Ce}_x\text{Sm}_y\text{SiO}_4$ ,  $\text{LiLn}_{1-x-y}\text{Ce}_x\text{Tb}_y\text{SiO}_4$  and  $\text{LiLn}_{1-x-y}\text{Ce}_x\text{Eu}_y\text{SiO}_4$  were prepared by solid state reaction from  $\text{Li}_2\text{CO}_3$ ,  $\text{Ln}_2\text{O}_3$  ( $\text{Ln} = \text{Y, La, Gd, or Lu}$ ),  $\text{SiO}_2$  and  $\text{CeF}_3$  and/or  $\text{Sm}_2\text{O}_3$ ,  $\text{Tb}_2\text{O}_3$  or  $\text{Eu}_2\text{O}_3$ . The mixture was fired for 8 h at 800 °C in Ar atmosphere. After this, samples were ground and fired again for 15 h in Ar atmosphere. The firing temperature in the last procedure varied depending on the dopant or the host lattice.

The crystal structures of  $\text{LiLnSiO}_4$  are known from the works by Blasse *et al* [14] and Nakayama *et al* [15]. The structures can be derived from that of  $\text{Ca}_2\text{SiO}_4$  by the substitution of  $2\text{Ca}^{2+} \rightarrow \text{Li}^+ + \text{Ln}^{3+}$ . Compounds with  $\text{Ln} = \text{La, Ce, \dots, Dy}$  are hexagonal [14, 15]. Compounds with  $\text{Ln} = \text{Ho, Er, \dots, Lu}$  and  $\text{Y}$  are orthorhombic. Eight oxygen atoms belonging to  $\text{SiO}_4$  tetrahedrons surround the  $\text{Ln}^{3+}$  ion in the form of a trigonal prism with two distant capping oxygens. The site has  $C_1$  point symmetry.

All the samples were checked by x-ray diffraction analysis and compared with the diffraction pattern known from Nakayama *et al* [15]. In the x-ray diffraction spectra of  $\text{LiYSiO}_4$  samples fired at 1075 °C in the second stage, lines from a parasitic phase were found and attributed to the  $\text{Y}_{4.67}(\text{SiO}_4)_3\text{O}$  phase. For the samples fired at the lower temperature of 1000 °C

these lines are absent. The latter can be explained by Li evaporation from the yttrium samples at temperatures higher than 1000 °C. Since  $\text{LiYSiO}_4$  and  $\text{LiLuSiO}_4$  are orthorhombic and the phases without Li are hexagonal, it became possible to distinguish the parasitic phase. For the  $\text{LiLuSiO}_4$  series the final firing temperature was 1150 °C and for the  $\text{LiYSiO}_4$  series 1000 °C.

X-ray excited emission spectra were recorded using an x-ray tube with a Cu anode operated at 35 kV and 25 mA. A combination of a vacuum monochromator (ARC VM504) and a photomultiplier tube (PMT) detect the light emitted from the sample. Excitation and emission measurements in the UV and visible region were performed with a QuantaMaster QM-1 spectrophotometer from Photon Technology International. Excitation spectra around 10 K were measured at the Deutsche Electronen Synchrotron (DESY) in Hamburg (Germany) at the Superlumi station of HASYLAB.

Thermal and photon stimulated luminescence measurements were carried out using an automated reader manufactured by Riso, Danish National Laboratory (Risø TL/OSL-DA-15A/B reader), which is equipped with a PM tube with bi-alkali photocathode (Thorn-EMI 9235QA). The reader is equipped with a  $^{90}\text{Sr}/^{90}\text{Y}$   $\beta$  source that produces a dose rate of 1 mGy  $\text{s}^{-1}$  in air at the sample position. TL measurements were performed in a nitrogen atmosphere.

The photo-stimulation spectrum was recorded utilizing a Xe flash lamp. Prior to the recording the samples are exposed to a relatively high radiation dose which fills all the charge traps. By scanning from long to short wavelengths, the trapped charges are optically excited from the traps, leading to short wavelength luminescence. During the entire recording only a fraction of the filled traps are emptied, thus preventing distortion of the recorded spectrum.

### 3. Results

#### 3.1. Optical properties

To determine the energy level location for all divalent lanthanides we need to locate the  $\text{Eu}^{2+}$  ground state and for all trivalent lanthanides the  $\text{Ce}^{3+}$  5d state relative to the bands of the host compound. This information together with the energy difference between the lowest 4f and lowest 5d states in  $\text{Ce}^{3+}$  and/or  $\text{Eu}^{2+}$  and the bandgap energy is sufficient to derive the level locations for all the other lanthanide ions [13].

In figure 1 the x-ray excited emission spectra of  $\text{LiLnSiO}_4:\text{Ce}$ ,  $\text{Sm}$  are presented. They consist of the known emission band of  $\text{Ce}^{3+}$  5d  $\rightarrow$  4f transitions with a maximum at 400 nm together with  $\text{Sm}^{3+}$  4f<sup>5</sup>  $\rightarrow$  4f<sup>5</sup> transitions in the range 550–800 nm [16, 17]. In the  $\text{Ce}^{3+}$  emission spectrum the transitions to the two  $^2\text{F}_{5/2}$  and  $^2\text{F}_{7/2}$  ground state components cannot be resolved due to spectral overlap.

The excitation spectra of  $\text{Ce}^{3+}$  emission in  $\text{LiYSiO}_4$  and  $\text{LiLuSiO}_4$  are shown in figure 2. The bands at 349, 315, 298 and 352, 316, 303 nm are attributed to transitions to the first three  $\text{Ce}^{3+}$  5d components in  $\text{LiYSiO}_4$  and  $\text{LiLuSiO}_4$  respectively. This attribution is confirmed by the decay time measurements of  $\text{Ce}^{3+}$  emission, shown in figure 3. The decay curves of  $\text{Ce}^{3+}$  emission excited at 302 and 320 nm have 30 ns decay time, which is typical for fast dipole allowed 5d  $\rightarrow$  4f emission.

Excitation and emission spectra of  $\text{LiYSiO}_4:\text{Eu}^{3+}$  measured at 10 K under synchrotron radiation are shown in figure 4. The excitation spectrum of  $\text{Eu}^{3+}$  emission at 610 nm shows a broad band starting at 280 nm with a plateau at 220 nm followed by a slight increase near 210 nm. When the sample is excited at 206 nm, two types of emissions can be observed in figure 4(b). The first is the typical sharp-line emission between 450 and 700 nm due to  $\text{Eu}^{3+}$  4f<sup>6</sup>  $\rightarrow$  4f<sup>6</sup> transitions and the second is a broad band at about 350 nm. The excitation

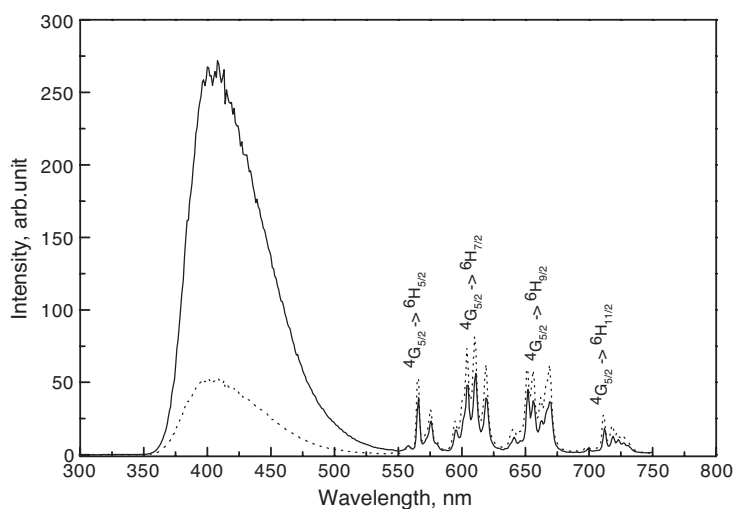


**Figure 1.** X-ray excited emission spectra of  $\text{LiLuSiO}_4:1\% \text{Ce}^{3+}, 0.2\% \text{Sm}^{3+}$  (solid curve) and  $\text{LiYSiO}_4:1\% \text{Ce}^{3+}, 0.2\% \text{Sm}^{3+}$  (dotted curve).

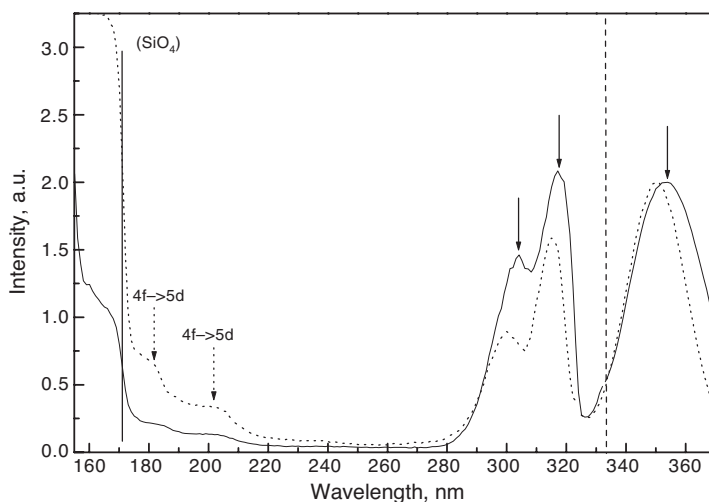


**Figure 2.** Excitation spectra of  $\text{Ce}^{3+}$  emission at 390 nm in  $\text{LiLuSiO}_4:1\% \text{Ce}^{3+}$  (solid curve) and  $\text{LiYSiO}_4:1\% \text{Ce}^{3+}$  (dotted curve). Measurements at shorter wavelengths than 335 nm were carried out at 10 K using synchrotron radiation. Measurements at longer wavelengths were carried out at room temperature using the spectrofluorometer. The bands indicated by solid arrows are attributed to the first three 5d bands of  $\text{Ce}^{3+}$ . The bands marked by dotted arrows are tentatively attributed to the remaining two 5d bands of  $\text{Ce}^{3+}$ .

spectrum of this 350 nm emission is shown in figure 4(a) and has a clear threshold at about 210 nm. It was verified that excitation at 225 nm causes only the  $4f^6 \rightarrow 4f^6$   $\text{Eu}^{3+}$  emission with total absence of the 350 nm emission. The nature of the defect responsible for the 350 nm emission is not known.

The edge at 210 nm is also clearly visible in the excitation spectrum of  $\text{Eu}^{3+}$  emission for  $\text{LiLuSiO}_4:\text{Eu}^{3+}$  in figure 5(b). We conclude that the excitation spectrum of  $\text{Eu}^{3+} 4f^6 \rightarrow 4f^6$  emission consists of the superposition of two bands. One is from the unknown defect that can

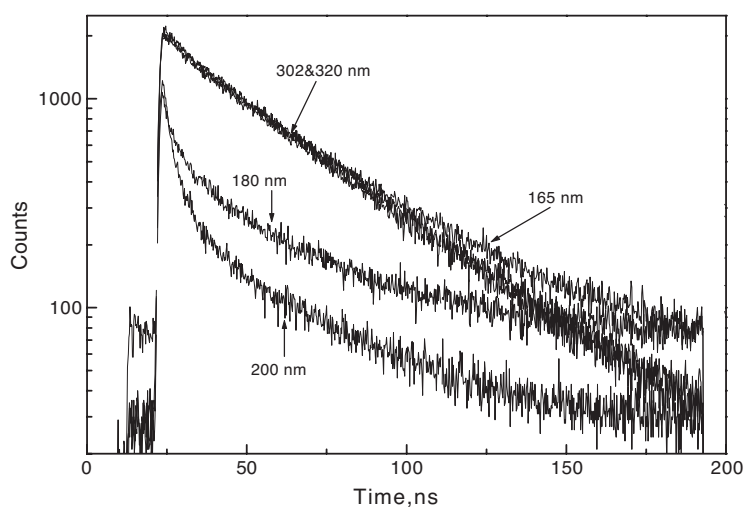


**Figure 3.** Decay time curves of  $\text{Ce}^{3+}$  emission at 390 nm in  $\text{LiLuSiO}_4:1\% \text{Ce}^{3+}$  excited at different wavelengths. The measurements were carried out using synchrotron radiation at 10 K.

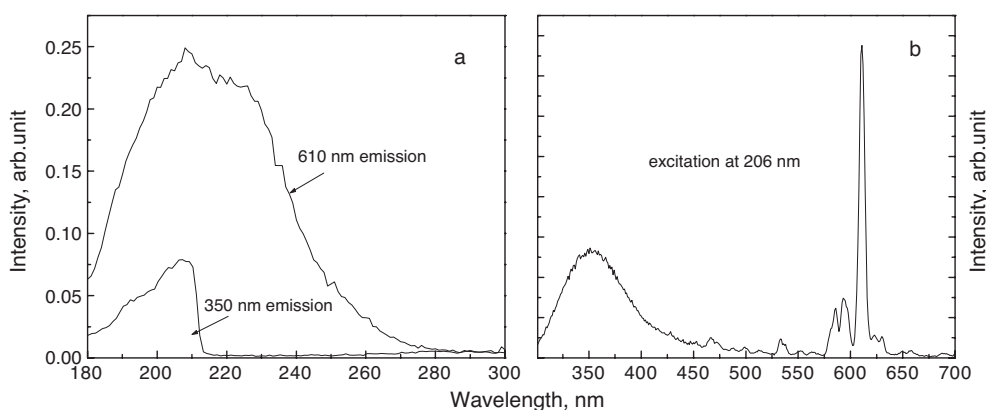


**Figure 4.** (a) Excitation spectrum of  $\text{Eu}^{3+}$  line emission at 610 nm and excitation spectrum of broad band 350 nm emission. (b) Emission spectrum of  $\text{LiYSiO}_4:1\% \text{Eu}^{3+}$  at 206 nm excitation. Measurements were carried out at 10 K using synchrotron radiation.

only be excited at wavelengths shorter than 210 nm and the other has been fitted by a Gaussian shaped broad band; see figure 5. We attribute this band to the charge transfer of an electron from the top of the valence band to  $\text{Eu}^{3+}$ .

### 3.2. Thermoluminescence properties

TL glow curves of  $\text{LiLuSiO}_4$  with different activators are shown in figure 6. For the samples doped with  $\text{Tb}^{3+}$  and  $\text{Ce}^{3+}$  there is a glow peak at 480 K. The peak position does not change with the type of activator. The emission during the TL readout at 480 K is due to Ce emission in  $\text{LiLuSiO}_4:\text{Ce}^{3+}$ , due to typical  $\text{Tb}^{3+} 4f^8 \rightarrow 4f^8$  emission in  $\text{LiLuSiO}_4:\text{Tb}^{3+}$ , and a superposition of both in  $\text{LiLuSiO}_4:\text{Ce}^{3+}, \text{Tb}^{3+}$ . Note that with 1% of  $\text{Sm}^{3+}$  doping in  $\text{LiLuSiO}_4$  the 480 K glow peak is drastically reduced.

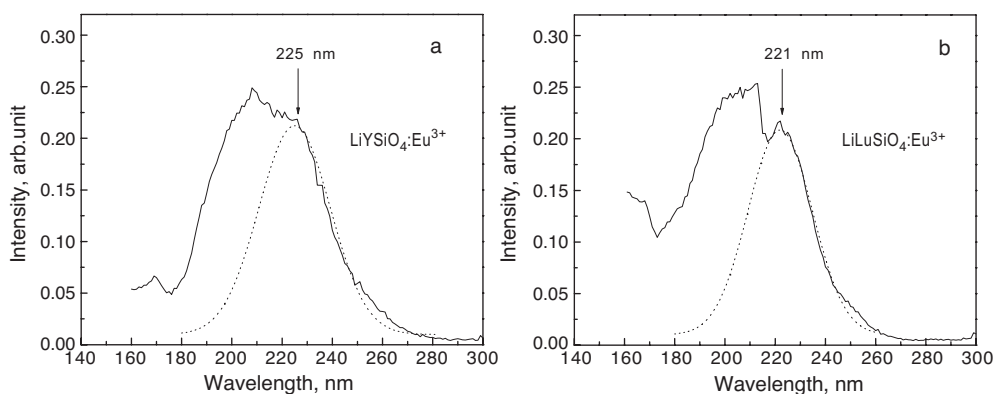


**Figure 5.** (a) Excitation spectrum of  $\text{Eu}^{3+}$  line emission at 610 nm in  $\text{LiYSiO}_4:1\%\text{Eu}^{3+}$ . (b) Excitation spectrum of  $\text{Eu}^{3+}$  line emission at 610 nm in the  $\text{LiLuSiO}_4:1\%\text{Eu}^{3+}$  sample. The dotted curves are Gaussian fits to the right long wavelength parts of the spectra. Measurements were carried out at 10 K using synchrotron radiation.

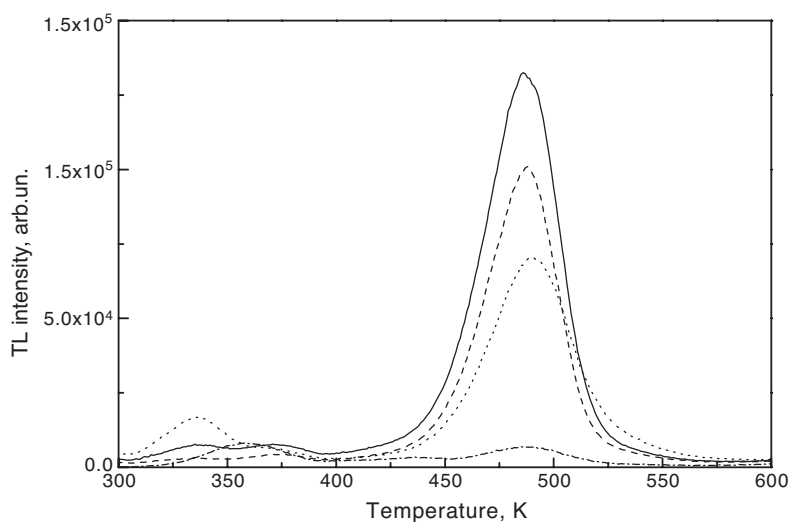


**Figure 6.** TL glow curves of  $\text{LiLuSiO}_4:1\%\text{Ce}^{3+}$  (dashed curve),  $\text{LiLuSiO}_4:0.5\%\text{Ce}^{3+}, 0.5\%\text{Tb}^{3+}$  (solid curve),  $\text{LiLuSiO}_4:0.5\%\text{Tb}^{3+}$  (dotted curve) and  $\text{LiLuSiO}_4:1\%\text{Sm}^{3+}$  (dash-dotted curve) after  $\beta$ -irradiation. The TL recording with a heating rate of  $1\text{ K s}^{-1}$  started 100 s after the end of the  $\beta$ -irradiation. All the samples were of the same shape and volume.

In figure 7 the TL glow curves of  $\text{LiLuSiO}_4:1\%\text{Ce}^{3+}, 0.2\%\text{Sm}^{3+}$  recorded at different waiting times after irradiation are plotted. The TL glow peak at 480 K has about the same intensity as that in  $\text{LiLuSiO}_4:1\%\text{Ce}^{3+}$  shown in figure 6. In addition to the 480 K glow peak a glow peak at 340 K is present. The traps responsible for this glow peak are emptied within 5 h waiting time. Measurements of the emission during thermal stimulation show that the emission of this glow peak originates only from  $\text{Ce}^{3+}$  centres.

In figure 8 the TL curves of  $\text{LiYSiO}_4:1\%\text{Ce}^{3+}, 0.2\%\text{Sm}^{3+}$  recorded at different waiting times after irradiation are shown. The low temperature peak is now positioned at 400 K and it is stable at room temperature. The 480 K glow peak in  $\text{LiLuSiO}_4:1\%\text{Ce}^{3+}, 0.2\%\text{Sm}^{3+}$  is

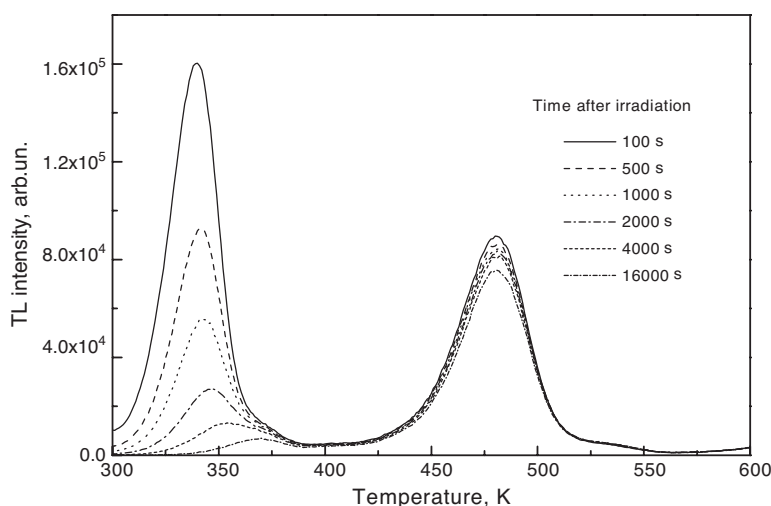


**Figure 7.** TL glow curves of  $\text{LiLuSiO}_4:1\% \text{Ce}^{3+}, 0.2\% \text{Sm}^{3+}$  recorded with a heating rate of  $1 \text{ K s}^{-1}$ . The recording started at different waiting times after the end of the  $\beta$ -irradiation.

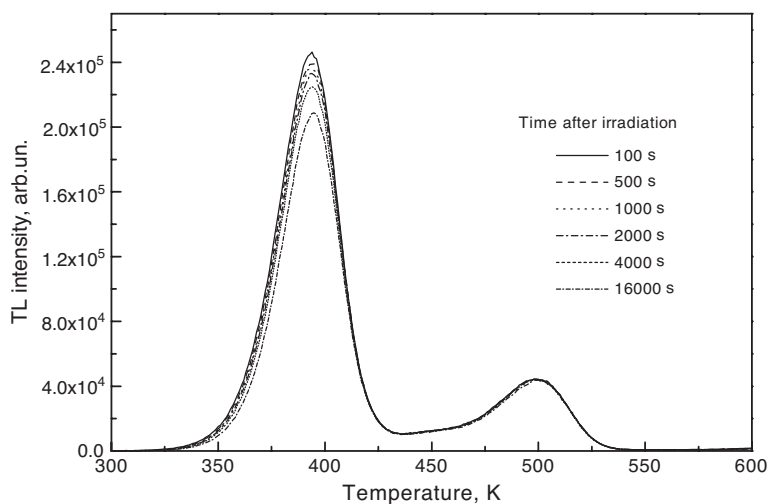


**Figure 8.** TL glow curves of  $\text{LiYSiO}_4:1\% \text{Ce}^{3+}, 0.2\% \text{Sm}^{3+}$  recorded with a heating rate of  $1 \text{ K s}^{-1}$ . The recording started at different waiting times after the end of the  $\beta$ -irradiation.

shifted 20 K to higher temperature in  $\text{LiYSiO}_4:1\% \text{Ce}^{3+}, 0.2\% \text{Sm}^{3+}$ . Intense glow peaks were not observed in  $\text{LiLuSiO}_4:\text{Ce}^{3+}, \text{Eu}^{3+}$  and  $\text{LiYSiO}_4:\text{Ce}^{3+}, \text{Eu}^{3+}$  samples.

To study the conditions required to empty the filled traps, photostimulation spectra using a Xe-flash lamp were recorded. Prior to the photostimulation the traps were filled by means of intense  $\beta$ -irradiation. During the photostimulation, the released charge carriers recombine on luminescence centres ( $\text{Ce}^{3+}$ ) and the resulting luminescence is detected. In figure 9 the photostimulation spectra of  $\text{LiLuSiO}_4:1\% \text{Ce}^{3+}, 0.2\% \text{Sm}^{3+}$  are plotted. They were recorded immediately (curve (a)) and two hours (curve (b)) after 20 min  $^{60}\text{Co}$ -irradiation with a dose rate of  $6 \text{ kGy h}^{-1}$ . The photostimulation curve of  $\text{LiLuSiO}_4:1\% \text{Ce}^{3+}, 0.2\% \text{Sm}^{3+}$  recorded immediately after irradiation represents the combined stimulation spectrum of the



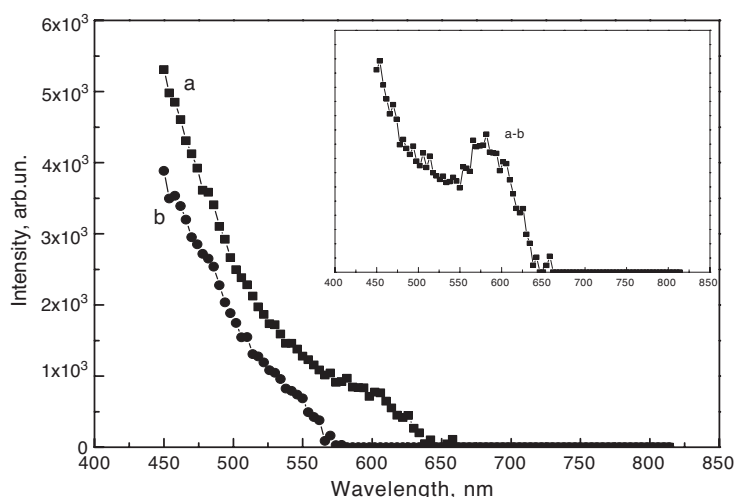


**Figure 9.** Photo-stimulation spectra of  $\text{LiLuSiO}_4:1\% \text{Ce}^{3+}, 0.2\% \text{Sm}^{3+}$  measured at 390 nm emission. Curve (a) was measured just after  $\beta$ -irradiation. Curve (b) was measured 2 h after  $\beta$ -irradiation. In the inset a difference between curve (a) and curve (b) is shown.

traps corresponding to TL glow peaks at 340 and 480 K. This curve starts at 650 nm and monotonically increases with photon energy with a plateau at about 580 nm (curve (a), figure 9). The photostimulation curve recorded two hours after irradiation has a threshold at 570 nm; see curve (b) in figure 9. As can be seen in figure 7 the TL peak at 340 K has almost completely disappeared two hours after the irradiation phase. Therefore, curve (b) in figure 9 represents the stimulation spectrum of trapped charge carriers corresponding exclusively to the TL glow peak at 480 K. By subtracting curve (b) from curve (a) one obtains the stimulation spectrum of trapped charge carriers responsible for the glow peak at 340 K as shown in the inset of figure 9. The same type of experiments were performed on  $\text{LiYSiO}_4:1\% \text{Ce}^{3+}, 0.2\% \text{Sm}^{3+}$  and the results are similar as for  $\text{LiLuSiO}_4:1\% \text{Ce}^{3+}, 0.2\% \text{Sm}^{3+}$ . We conclude that photons between 550 and 650 nm are efficient in liberating the charge carriers from the traps responsible for the 480 K glow peak in figure 7.

#### 4. Discussion

The excitation spectra of  $\text{Ce}^{3+}$  emission in figure 2 show a steep increase at wavelengths shorter than 171 nm for both  $\text{LiLuSiO}_4:\text{Ce}^{3+}$  and  $\text{LiYSiO}_4:\text{Ce}^{3+}$ . This threshold value is comparable with absorption edges at 165 nm in  $\text{Li}_2\text{CaSiO}_4$  and at 177 nm in  $\text{Lu}_2\text{Si}_2\text{O}_7$  [18, 19]. They are attributed to the absorption by the  $\text{SiO}_4^{4-}$  groups. We conclude that the levels of the silicate groups form the bottom of the conduction band, and the optical bandgaps of  $\text{LiLuSiO}_4$  and  $\text{LiYSiO}_4$  are at 7.25 eV.

The spin-orbit interaction splits the 5d configuration of free  $\text{Ce}^{3+}$  into two  $^2\text{D}_{3/2}$  and  $^2\text{D}_{5/2}$  levels. In  $\text{LiLuSiO}_4$  and  $\text{LiYSiO}_4$  with sites of  $C_1$  point symmetry they are further split by the crystal field into five distinct 5d states [18]. The first three bands in the excitation spectra in figure 2 are certainly due to the  $\text{Ce}^{3+}$  5d states. With increasing energy, we will denote these states and bands as 5d<sub>1</sub>, 5d<sub>2</sub> and 5d<sub>3</sub>. The question arises of where the other two 5d<sub>4</sub> and 5d<sub>5</sub> bands are located. For  $\text{Ce}^{3+}$  in a trigonal prism coordination of six oxygen atoms at average distance of 232 pm a total splitting between the lowest 5d<sub>1</sub> and highest 5d<sub>5</sub> state of about 3.0 eV is expected [18, 19]. We therefore anticipate the 4f–5d<sub>5</sub> excitation around 190 nm.

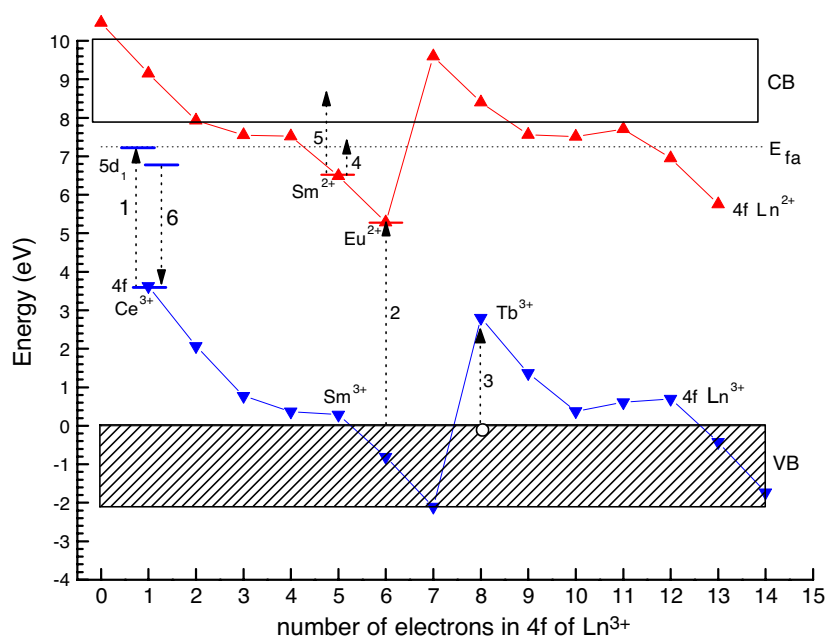


**Figure 10.** Scheme of the 4f ground state energy positions of lanthanide ions relative to the valence and conduction bands in  $\text{LiYSiO}_4$  and  $\text{LiLuSiO}_4$ .  $E_{fa}$  is the threshold energy for the fundamental absorption. The top of the valence band is defined as the zero of energy. Arrow 1 shows the 4f–5d<sub>1</sub> transition and arrow 6 the Stokes shifted emission. Curve 4f Ln<sup>3+</sup> connects the ground state energies of the trivalent lanthanides. The number of electrons in the 4f ground state of Ln<sup>3+</sup> identifies the type of lanthanide ion along the horizontal axis. Arrow 2 is the energy of charge transfer from the valence band to Eu<sup>2+</sup>. It forms the basis to draw the curve labelled 4f Ln<sup>2+</sup> that connects the ground state energies of the divalent lanthanides. Arrow 3 illustrates hole trapping by Tb<sup>3+</sup>, arrow 4 represents the observed activation energy for thermally stimulated and arrow 5 for optically stimulated electron release from Sm<sup>2+</sup>.

(This figure is in colour only in the electronic version)

In the excitation spectra of Ce<sup>3+</sup> emission in figure 2, two relatively broad bands at 203 and 182 nm are present. Decay curves of Ce<sup>3+</sup> emission when excited in these two bands are fast but clearly non-exponential; see figure 3. An initial decay that is faster than the intrinsic lifetime of the Ce<sup>3+</sup> 5d state is followed by a very slow component with a decay constant of several microseconds. The decay behaviour is evidently different from excitation into 5d<sub>1</sub>, 5d<sub>2</sub> and 5d<sub>3</sub>. We tentatively assign these two bands to the excitation of the 5d<sub>4</sub> and 5d<sub>5</sub> states of Ce<sup>3+</sup> because they do lead to Ce<sup>3+</sup> 5d–4f emission and their energies are near the anticipated value. The low excitation intensity and deviating decay behaviour is then attributed to a location of the 5d<sub>4</sub> and 5d<sub>5</sub> states inside the conduction band. The 5d → 4f emission is then partly quenched by auto-ionization processes of the 5d electron to conduction band states. The quenching explains both the fast decay component in figure 3 and the low intensity of the 5d<sub>4</sub> and 5d<sub>5</sub> excitation bands in figure 2. The presence of the μs slow Ce<sup>3+</sup> emission component in figure 3 is then attributed to re-trapping of the auto-ionized electron by Ce<sup>4+</sup> followed by 5d–4f emission.

With the experimental data presented we have now sufficient information to estimate the location of lanthanide energy levels in  $\text{LiLnSiO}_4$ . Because the properties of the host compounds  $\text{LiYSiO}_4$  and  $\text{LiLuSiO}_4$  are very similar we will make no distinction between the two when constructing the energy level diagram as shown in figure 10. In figure 10 the

onset of fundamental absorption is drawn at  $E_{fa} = 7.25$  eV corresponding to the 171 nm threshold in figure 2. At this energy bound electron–hole pairs are excited near the  $\text{SiO}_4$ -group absorption band of the host lattice. Assuming an electron–hole binding energy of 0.6–0.7 eV, the bottom of the conduction band is estimated at around 7.9 eV. From the discussion in the previous paragraph we conclude that the  $5d_4$  and  $5d_5$   $\text{Ce}^{3+}$  bands are located above the bottom of the conduction band. Furthermore, the  $5d_1$  state is estimated at least 0.7 eV below the conduction band bottom because otherwise the  $5d$ – $4f$  emission would be thermally quenched during readout of the 480 K TL glow peak in figure 7.

In figure 10 we have chosen to position the  $5d_1$  band of  $\text{Ce}^{3+}$  at 7.2 eV and from this (see arrow 1) the  $\text{Ce}^{3+}$  ground state is found at 3.6 eV above the top of the valence band. However, we could equally well have chosen the  $5d_4$  state at the bottom of the conduction band around 8 eV leading to a  $4f$  ground state 2 eV above the valence band. This places the  $\text{Ce}^{3+}$  ground state at  $2.8 \pm 0.8$  eV; the true position is still undetermined.

The excitation spectrum of  $\text{Eu}^{3+}$  emission in figure 5 is a superposition of two bands. We attributed the excitation band in figure 5 fitted with Gaussian functions to the CT absorption bands of  $\text{Eu}^{3+}$ . The values of  $\text{Eu}^{3+}$  CT energies in  $\text{LiLuSiO}_4$  and  $\text{LiYSiO}_4$  were reported earlier by Blasse *et al* [14] at 5.3 eV for both compounds. However, our results reveal that the CT absorption band of  $\text{Eu}^{3+}$  in  $\text{LiLuSiO}_4$  and  $\text{LiYSiO}_4$  is at about 5.5–5.6 eV.

The data on CT energies of different lanthanides in a large number of compounds were collected by one of us, and a general method to determine the CT energies of all the other lanthanides relative to that of  $\text{Eu}^{3+}$  was established [13, 20]. The CT energy to  $\text{Eu}^{3+}$  is equal to the energy difference between the  $\text{Eu}^{2+}$  ground state and the top of the valence band. This is illustrated by arrow 2 in figure 10. From the location of the  $\text{Eu}^{2+}$  ground state the location of the lowest  $4f$  state for each other divalent lanthanide ion can be constructed. This is illustrated by the curve labelled  $4f \text{Ln}^{2+}$  in figure 10. With a similar method [13] we have drawn the ground state energies for the trivalent lanthanides (the curve labelled  $4f \text{Ln}^{3+}$ ) based on the location of the  $4f$  ground state of  $\text{Ce}^{3+}$ .

Although the absolute positions of the trivalent lanthanide ground states are still subject to  $\pm 0.8$  eV systematic error, the relative variations indicated by the curve labelled  $4f \text{Ln}^{3+}$  are more accurate. The ground state of  $\text{Tb}^{3+}$  is for example always  $0.8 \pm 0.1$  eV below that of  $\text{Ce}^{3+}$  [13]. With these error margins it is quite certain that the ground state of both  $\text{Ce}^{3+}$  and  $\text{Tb}^{3+}$  are located above the valence band. The systematic error in the location of the divalent lanthanides is estimated at  $\pm 0.4$  eV. It is also clear that the  $\text{Ce}^{2+}$  and  $\text{Tb}^{2+}$  ground states are inside the conduction band. From the scheme in figure 10 we now conclude that  $\text{Ce}^{3+}$  and  $\text{Tb}^{3+}$  cannot trap electrons but they are efficient hole traps; see for example arrow 3 in figure 10. We also conclude that  $\text{Eu}^{3+}$  and  $\text{Sm}^{3+}$  are stable electron traps, because the ground states of  $\text{Eu}^{2+}$  and  $\text{Sm}^{2+}$  are well below the conduction band.

With the help of the level diagram we can explain quantitatively the TL results.  $\text{LiLuSiO}_4$  doped with  $\text{Ce}^{3+}$  and/or  $\text{Tb}^{3+}$  shows an intense TL glow peak at 480 K in figure 6. Figure 10 indicates that  $\text{Ce}^{3+}$  and  $\text{Tb}^{3+}$  ions are hole traps and therefore the electron must be trapped somewhere else. We also know that the recombination during TL readout occurs at Ce and Tb, leading to  $\text{Ce}^{3+}$  and  $\text{Tb}^{3+}$  emission. We now attribute the glow peak at 480 K to release of electrons trapped at intrinsic defects of the host followed by recombination at  $\text{Ce}^{4+}$  or  $\text{Tb}^{4+}$ . This is confirmed by the absence of an intense 480 K TL glow peak in  $\text{LiLuSiO}_4:1\% \text{Sm}^{3+}$ , see figure 6. According to the scheme of figure 10,  $\text{Sm}^{3+}$  is not a stable hole trap at room temperature. In the absence of a stable hole trap as with  $\text{Ce}^{3+}$  or  $\text{Tb}^{3+}$  there is not an efficient filling of the electron traps either, leading to low 480 K glow peak intensity.

In  $\text{LiLnSiO}_4$  doubly doped with  $\text{Ce}^{3+}$  and  $\text{Sm}^{3+}$  an extra intense glow peak appears at 340 K for  $\text{Ln} = \text{Lu}$  and 400 K for  $\text{Ln} = \text{Y}$  in figures 7 and 8, respectively. We conclude

that co-doping with Sm<sup>3+</sup> ions provides an extra electron trap. After electron capture, divalent samarium is created, with its ground state located below the conduction band in agreement with the scheme in figure 10. Upon thermal stimulation the electrons released from Sm<sup>2+</sup> recombine with Ce<sup>4+</sup> centres. The resulting Ce<sup>3+</sup> luminescence gives rise to the TL glow peak at 340 K in LiLuSiO<sub>4</sub> or 400 K in LiYSiO<sub>4</sub>.

The nature of the intrinsic lattice defects responsible for electron trapping and the high temperature peak was further investigated. We tested whether oxygen vacancies may play the role of electron trap in the studied materials. Argon atmosphere was used during synthesis to prevent formation of tetravalent Ce. One expects that additional firing of the material in oxygen atmosphere will lead to higher content of Ce<sup>4+</sup> and lower content of oxygen vacancies. We annealed LiLuSiO<sub>4</sub>:Ce<sup>3+</sup>, Sm<sup>3+</sup> and LiYSiO<sub>4</sub>:Ce<sup>3+</sup>, Sm<sup>3+</sup> at 900 °C for 4 h. As a result, the 480 K high temperature glow peak for LiLuSiO<sub>4</sub> in figure 7 and the 500 K glow peak for LiYSiO<sub>4</sub> in figure 8 disappear, and the intensities of the low temperature glow peaks are halved. The absence of the high temperature glow peaks is attributed to a complete removal of oxygen vacancies. The decrease of the low temperature TL glow peaks can be caused by partial conversion of Ce<sup>3+</sup> into Ce<sup>4+</sup>, which leads to a decrease of the number of available luminescent and hole trapping centres.

The TL mechanism associated with the low temperature glow peak was investigated in more detail. The glow curves in figures 7 and 8 show that the low temperature glow peak is shifted by  $\Delta T = 60$  K to higher temperature in LiYSiO<sub>4</sub> as compared to LiLuSiO<sub>4</sub>. These two glow peaks were fitted assuming Randall–Wilkins first order kinetics [1]. The activation energy  $E_T$  and the attempt-to-escape frequency  $s$  are the two parameters of the fit. Since the nature of the recombination mechanism is the same in LiLuSiO<sub>4</sub>:Ce<sup>3+</sup>, Sm<sup>3+</sup> and LiYSiO<sub>4</sub>:Ce<sup>3+</sup>, Sm<sup>3+</sup>, we assumed the same frequency factor for both compounds. The fitting procedure yields  $s = 10^8$  s<sup>-1</sup> and  $E_T = 0.82$  eV for LiLuSiO<sub>4</sub>:Ce<sup>3+</sup>, Sm<sup>3+</sup> and  $E_T = 0.95$  eV for LiYSiO<sub>4</sub>:Ce<sup>3+</sup>, Sm<sup>3+</sup>. Thus the depth of the Sm electron trap in LiYSiO<sub>4</sub> is only 0.1 eV deeper than in LiLuSiO<sub>4</sub>. Such small energy differences cannot be revealed with the techniques used in constructing the scheme of figure 10.

The magnitude of  $E_T$  is indicated with arrow 4 in figure 10. Although it does not end above the bottom of the conduction band, we still regard this as a confirmation that the recombination mechanism upon thermal stimulation occurs via release of an electron from Sm<sup>2+</sup> to the conduction band. The difference from the bottom of the conduction band still falls within the error margins of about 0.4 eV in the location of energy levels. Furthermore, phonon assisted transitions may reach conduction band levels at different points in  $k$ -space than photon transitions, and one may not exclude that the conduction band bottom for phonon transition is at lower energy than that for photon transitions. The results also show that a trap depth difference of 0.1 eV has a significant effect on the TL peak position and consequently on fading characteristics.

In the photostimulation spectrum of figure 9 the energy of the band at about 2.1 eV (580 nm) is higher than the energy difference between the Sm<sup>2+</sup> ground state and the bottom of the conduction band; see arrow 5. The band at 580 nm is attributed to Sm<sup>2+</sup> 4f → 5d transitions, and not to direct 4f → CB transitions. Thus the recombination mechanism upon photo-stimulation occurs via excitation of Sm<sup>2+</sup> to a 5d state with subsequent ionization and electron capture by Ce<sup>4+</sup>.

The absence of a TL signal in LiLuSiO<sub>4</sub>:Ce<sup>3+</sup>, Eu<sup>3+</sup> and LiYSiO<sub>4</sub>:Ce<sup>3+</sup>, Eu<sup>3+</sup> can also be explained with the scheme in figure 10. The position of the Eu<sup>2+</sup> ground state is at 1.2 eV lower energy than that of Sm<sup>2+</sup>, and Eu<sup>3+</sup> provides a more than 2 eV deep trap. This means that a possible related glow curve will be situated at high temperature, probably well above 600 K, where most likely the Ce<sup>3</sup> emission is already thermally quenched.

## 5. Summary

The possibility of controlled creation of electron- and hole-trapping centres by activating an inorganic material with appropriate Ln<sup>3+</sup> ions was demonstrated. The depth of electron traps due to trivalent lanthanides can be derived from the charge transfer absorption energy of any lanthanide and the value of the bandgap energy. As an example, the storage and recombination mechanism in lithium lutetium and lithium yttrium silicates doped with Ce<sup>3+</sup> and Sm<sup>3+</sup> was investigated. The derived values of electron trap depth energies obtained from spectroscopic and thermoluminescence experiments are in good agreement.

## Acknowledgments

These investigations were supported by the Netherlands Technology Foundation (STW), by IHP contract HPRI-CT-1990-00040 of the European Commission and by a van Gogh subsidy from the Netherlands Organization for Scientific Research (NWO). The authors thank Dr A Kahn-Harari for her considerable assistance in sample synthesis.

## References

- [1] Chen R and McKeever S W S 1997 *Theory of Thermoluminescence and Related Phenomena* (Singapore: World Scientific)
- [2] Chakrabarti K, Mathur V K and Rhodes J F 1988 *J. Appl. Phys.* **64** 1363
- [3] Tamura Y and Shibukawa A 1993 *Japan. J. Appl. Phys.* **32** 3187
- [4] Tamura Y and Mathur V K 1994 *Japan. J. Appl. Phys.* **33** 4640
- [5] Zhang J G, Eklund P C and Hua Z L 1988 *J. Appl. Phys.* **64** 1363
- [6] Zhi H, Yong-sheng W and Li S 2001 *J. Phys.: Condens. Matter* **13** 3665
- [7] Wu J, Newman D and Viney I 2001 *J. Lumin.* **99** 237
- [8] Chakrabarti K, Mathur V K and Thomas L A 1989 *J. Appl. Phys.* **65** 2021
- [9] Keller S P, Mapes J F and Cheroff G 1957 *Phys. Rev.* **108** 663
- [10] Keller S P and Pettit G D 1958 *Phys. Rev.* **111** 1533
- [11] Robins L and Tuchman J A 1998 *Phys. Rev. B* **57** 12094
- [12] Thiel C W, Cruguel H and Sun Y 2001 *J. Lumin.* **94/95** 1
- [13] Dorenbos P 2003 *J. Phys.: Condens. Matter* **15** 8417
- [14] Blasse G and Brill A 1967 *J. Inorg. Nucl. Chem.* **29** 2231
- [15] Nakayama S and Sakamoto M 1992 *J. Ceram. Soc. Japan* **100** 867
- [16] Knitel M J, Dorenbos P, Combes C M, Andriessen J and van Eijk C W E 1996 *J. Lumin.* **69** 325
- [17] Sidorenko A V, Bos A J J, Dorenbos P, van Eijk C W E, Kahn-Harari A, Rodnyi P A and Viana B 2005 *Nucl. Instrum. Methods* **537** 81
- [18] Dorenbos P, Pierron L, Dinca L, van Eijk C W E, Kahn-Harari A and Viana B 2003 *J. Phys.: Condens. Matter* **15** 511
- [19] Dorenbos P 2001 *Phys. Rev. B* **64** 125117
- [20] Dorenbos P 2005 *J. Lumin.* **111** 89